NeuroImage 252 (2022) 119014

Contents lists available at ScienceDirect

NeuroImage

journal homepage: www.elsevier.com/locate/neuroimage

A novel MRI-based quantitative water content atlas of the human brain

N. Jon Shah[a,b,c,d,#,*], Zaheer Abbas[a,c,#], Dominik Ridder[a], Markus Zimmermann[a], Ana-Maria Oros-Peusquens[a]

[a] Institute of Neuroscience and Medicine – 4, Forschungszentrum Juelich GmbH, Juelich, Germany
[b] Institute of Neuroscience and Medicine – 11, Forschungszentrum Juelich GmbH, Juelich, Germany
[c] Department of Neurology, Faculty of Medicine, RWTH Aachen University, Aachen, Germany
[d] JARA – BRAIN – Translational Medicine, RWTH Aachen University, Aachen, Germany

A B S T R A C T

The measurement of quantitative, tissue-specific MR properties, e.g., water content, longitudinal relaxation time (T_1) and effective transverse relaxation time (T_2^*), using quantitative MRI at a clinical field strength (1.5 T to 3T) is a well-explored topic. However, none of the commonly used standard brain atlases, such as MNI or JHU, provide quantitative information. Within the framework of quantitative MRI of the brain, this work reports on the development of the first quantitative brain atlas for tissue water content at 3T. A methodology to create this quantitative atlas of *in vivo* brain water content based on healthy volunteers is presented, and preliminary, practical examples of its potential applications are also shown.

Established methods for the fast and reliable measurement of the absolute water content were used to achieve high precision and accuracy. Water content and T_2^* were mapped based on two different methods: an intermediate-TR, two-point method and a long-TR, single-scan method. Twenty healthy subjects (age 25.3 ± 2.5 years) were examined with these quantitative imaging protocols. The images were normalised to MNI stereotactic coordinates, and water content atlases of healthy volunteers were created for each method and compared. Regions-of-interest were generated with the help of a standard MNI template, and water content values averaged across the ROIs were compared to water content values from the literature.

Finally, in order to demonstrate the strength of quantitative MRI, water content maps from patients with pathological changes in the brain due to stroke, tumour (glioblastoma) and multiple sclerosis were voxel-wise compared to the healthy brain.

The water content atlases were largely independent of the method used to acquire the individual water maps. Global grey matter and white matter water content values between the methods agreed with each other to within 0.5 %. The feasibility of detecting abnormal water content in the brains of patients based on comparison to a healthy brain water content atlas was demonstrated.

In summary, the first quantitative water content brain atlas *in vivo* has been developed, and a voxel-wise assessment of pathology-related changes in the brain water content has been performed. These results suggest that qMRI, in combination with a water content atlas, allows for a quantitative interpretation of changes due to disease and could be used for disease monitoring.

1. Introduction

Improving healthcare and education have led to an increasingly ageing population and, therefore, to an increased need for diagnostic tools and therapies. For example, instances of neurodegenerative diseases, such as Parkinson's disease and Alzheimer's disease, are rapidly increasing and morphometric methods to perform voxel-wise comparisons of healthy and diseased brains are common tools in clinical neuroscience to help assess and understand these diseases (Ashburner and Friston, 2000; Gaser, 2005; Good et al., 2001; Mechelli et al., 2004; Mechelli et al., 2005; Wright et al., 1995). The approach of defining healthy standard brain atlases as a basis for comparison with pathological brains has a long history. Following on from the dubious approaches of phrenology in the early 19th century, many scientific approaches to map the human brain have been developed (Broca, 1861; Brodmann, 1905, 1909). Currently, the use of such standard brain atlases is well established in the mapping community, but none of the commonly utilised standard brains or atlases (Mandal et al., 2012; Mazziotta et al., 1995; Talairach and Tournoux, 1988) provide quantitative information. "Standard brains", such as MNI305, a brain template from the Montreal Neurological Institute (MNI), reflect average neuroanatomy and provide the basis for a growing and evolving digital brain atlas (Collins et al., 1994; Evans A.C., 1993). These allow for a good comparison of parameters such as structure and volume, which can easily be derived by automated methods such as voxel-based morphometry (VBM) (Ashburner and Friston, 2000; Draganski et al., 2004; Good et al., 2001; Mechelli et al., 2004; Mechelli et al., 2005).

The hydrogen nucleus, the proton, is the nucleus of choice in the vast majority of MRI measurements due to its high abundance in biological tissue and its inherently high sensitivity for MR imaging. As most of the protons detectable with standard MR sequences are in tissue water, the proton magnetisation density (PD), which is the basis of MRI signal

* Corresponding author at: Institute of Neuroscience and Medicine (INM-4) Forschungszentrum Jülich, 52425, Jülich
E-mail address: n.j.shah@fz-juelich.de (N.J. Shah).
# Equal Contribution

https://doi.org/10.1016/j.neuroimage.2022.119014.
Received 23 December 2020; Received in revised form 8 February 2022; Accepted 17 February 2022
Available online 22 February 2022.

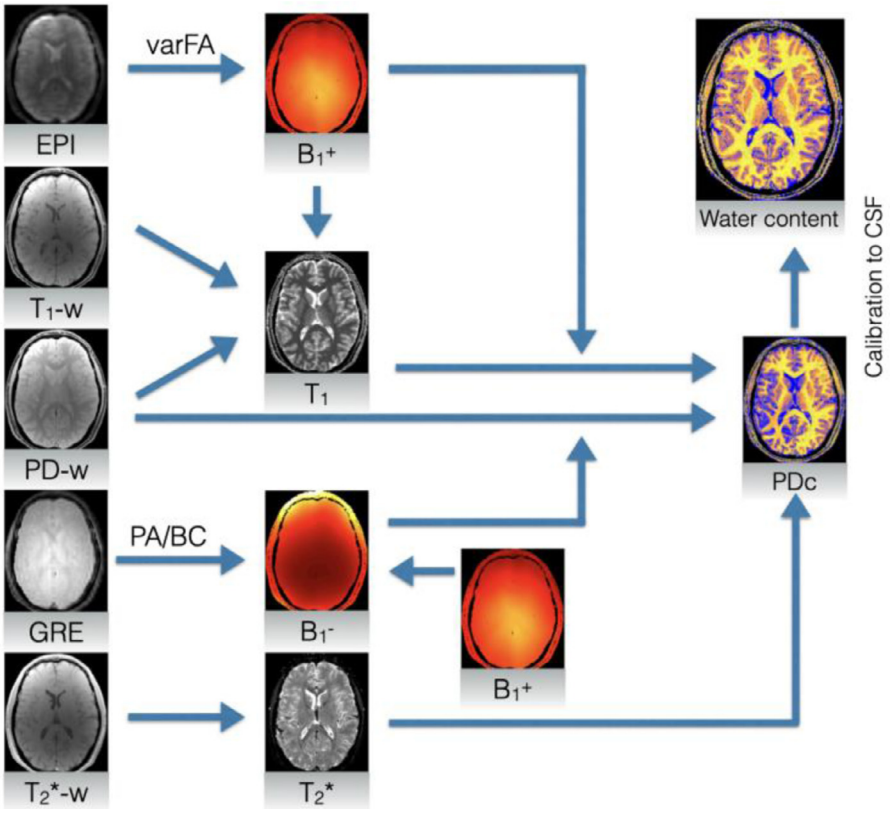

Figure 1. Graphical representation of the processing steps involved in the estimation of the water content using Method A.

and contrast, is often directly referred to as the water content of tissue; however, the often-employed notation, PD, refers only to the density of free protons in tissue water but does not include the MR-invisible bound protons (such as protons bound to macromolecules). Usually, water content of tissue is expressed in percentage units (Bloembergen, 1948) as the percentage of the water concentration in tissue with respect to pure water. In human white matter, for example, this is approximately 70% (Shah et al., 2001; Steinhoff et al., 2001; Tofts, 2003). By employing MR sequences with short echo times (TE) and long repetition times (TR), the MR-visible proton density can be measured since it is directly proportional to the measured MR signal strength. When the dominant contribution of the MR signal intensity is due to the protons in water molecules, the proportionality can be used to quantify the absolute water content in tissue if hardware imperfections have been properly corrected (Neeb and Shah, 2006; Tofts, 2003).

In recent years, novel quantitative MRI (qMRI) approaches have gained attention, and, especially for human brain imaging, qMRI is an attractive methodology to study pathological changes in the brain. Compared to conventional *qualitative* (i.e. non-quantitative) MRI, qMRI provides an unbiased measurement method and allows for more straightforward statistical modelling. By applying qMRI correctly, large national or even international multi-centre studies can be more directly compared. Furthermore, longitudinal studies for the precise evaluation of disease progression and monitoring become more amenable. In particular, degenerative and chronic diseases such as multiple sclerosis (MS), which has an onset in the early age ranges of life, can be much more accurately monitored and investigated in order to better understand, e.g., the correlation of lesion burden and physical disabilities, and especially long-term lesion behaviour and lesion differentiation. Quantitative measures of relaxation parameters, such as T_1 and/or T_2, as well as free water content, could provide a good basis for the detection of cerebral abnormalities in many diseases. Potentially, earlier detection might be facilitated using qMRI rather than with standard imaging methods, as many significant confounding effects afflicting conventional approaches are explicitly corrected in qMRI (Tofts, 2003).

More recently, qMRI, focussing on water content measurements, has been used to investigate several pathologies, including hepatic encephalopathy (Shah et al., 2008), tumour-generated oedema (Oros-Peusquens et al., 2014) and chronic kidney disease and haemodialysis (Reetz et al., 2015). Initial successful investigations using lower fields (1.5T) resulted in a significant amount of work (Neeb and Shah, 2006; Neeb et al., 2006a, b; Neeb, 2004; Shah et al., 2008) to overcome the failure of the reciprocity principle observed at higher fields, i.e., at 3T (Abbas et al., 2014; Abbas et al., 2015; Gras et al., 2013; Volz et al., 2012a) and above. More recently, work by Oros-Peusquens et al. (Oros-Peusquens et al., 2019) and Abbas et al. (Abbas et al., 2014) has shown how inhomogeneities arising from the coil sensitivity can be overcome. This facilitates quantitative water content measurement in the brain with a high contrast-to-noise (CNR) ratio, whilst maintaining accuracy even at 3T (Abbas et al., 2015). Considering recent progress in qMRI, it is all the more surprising to note the complete absence of quantitative water content atlases; in this work, this omission is addressed.

In order to demonstrate the strengths of tissue water content atlas, selected patient cases are presented, illustrating different diseases, which are known to lead to changes in the water content of the brain. The work herein describes the development of a quantitative water content brain atlas and its voxel-based comparison to the water content maps of a circumscribed number of patients; a full study of lesion water content in these patients is ongoing and is outside the scope of this manuscript.

2. Methods

2.1. Participants

All measurements were carried out on a 3 T Siemens Magnetom Tim-Trio scanner (Siemens Healthineers, Erlangen, Germany) using a

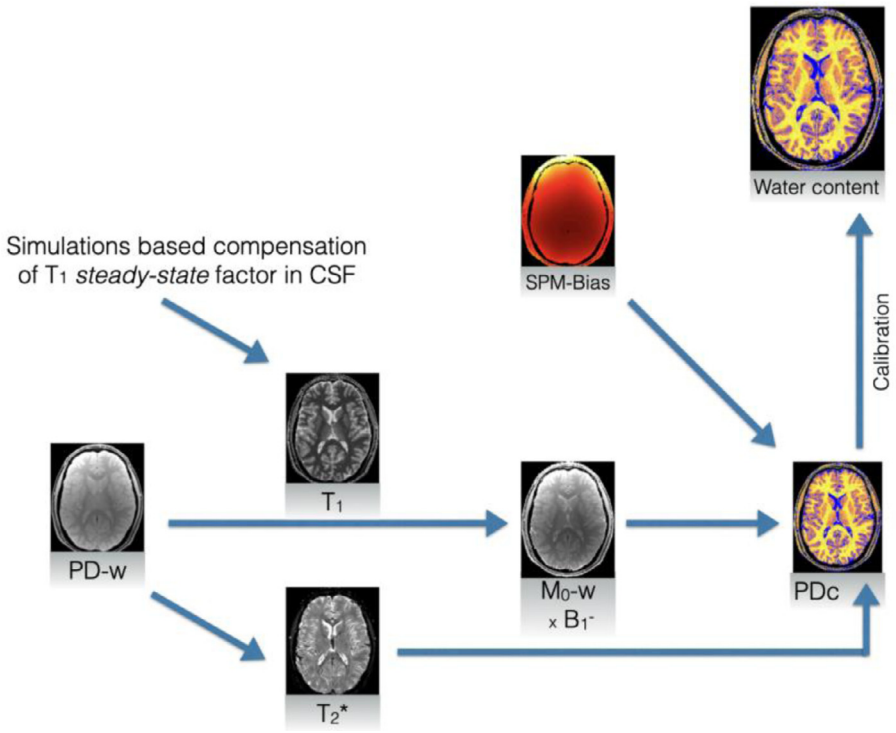

Figure 2. Schematic diagram of the processing steps for water content imaging using Method B.

multi-slice, multi-echo RF-spoiled gradient-echo (GRE) sequence. Radiofrequency (RF) excitation was achieved using the body coil, and a 32-channel phased-array receive head coil, as provided by the manufacturer, was used for signal reception. The study was approved by the local ethics committee and was conducted according to the declaration of Helsinki.

2.1.1. Healthy volunteers

Twenty right-handed, healthy male subjects (age 25.3 ± 2.5 years, age range 21.3 to 29.5 years) were recruited for the study. Each participant completed a screening questionnaire prior to the MR examination. Excessive alcohol or tobacco consumption and neurological disorders were criteria for rejection. This study was performed with the approval of the local ethics committee, and all participants gave prior, informed consent in writing.

2.1.2. Patients

Patients suffering from stroke (male, age 82 years), brain tumour (glioblastoma, male, 32 years) or multiple sclerosis (male, 38 years) went through similar imaging protocols as the healthy volunteers.

2.2. MRI data acquisition

Quantitative cerebral water content was measured using recently validated methods (Abbas et al., 2014; Abbas et al., 2015; Oros-Peusquens et al., 2014 Oros-Peusquens et al., 2019). MR-visible proton density was estimated (Abbas et al., 2014; Abbas et al., 2015; Gras et al., 2013; Neeb and Shah, 2006; Neeb et al., 2006b; Shah et al., 2008) to reflect the free water content (FW) present in the tissue (Tofts, 2003), and image acquisition was performed using two methods: intermediate TR method (Method A) and long TR method (Method B). The two methods were used and their atlases compared in order to demonstrate the generality of the quantitative water content atlas.

The data analysis steps for protocols A and B are schematically depicted in Figures 1 and 2, and a detailed description of the sequences, acquisition parameters and estimation of water content is provided in Table 1 and in Appendix A.

All healthy subjects were examined with the aforementioned quantitative imaging protocols using the following parameters:

- (Method A) Intermediate TR Method 64 slices; 1 mm in-plane resolution; 2 mm slice thickness (slice gap free acquisition); acquisition time = 13:50 minutes.
- (Method B) Long TR Method 57 slices; 1.04 mm in-plane resolution; 1.50 mm slice thickness (1mm slice gap); acquisition time = 7:30 minutes.

Following the water content protocol, a high-resolution 1 mm isotropic T_1-weighted image was obtained using a magnetisation-prepared rapid gradient-echo sequence (MPRAGE) to facilitate the transformation of the quantitative data into MNI space.

2.3. In vivo water content acquisition and data analysis

The graphical pipeline shown in Figure 1 summarises the data analysis steps for the calculation of the water content maps from Method A. The workflow for Method A is similar to that originally presented by Neeb et al. in 2006 (Neeb et al., 2006b); a detailed explanation of each step used in processing data from Method A can be found in Abbas et al. (Abbas et al., 2014).

The graphical pipeline shown in Figure 2 summarises the data analysis steps for the calculation of the water content maps from Method B. A detailed explanation of each step used in processing data from Method B can be found in Oros-Peusquens et al. (Oros-Peusquens et al., 2014).

The masks for 'normal' tissue classes: white matter (WM), grey matter (GM) and cerebrospinal fluid (CSF) were generated from the T_1-weighted MPRAGE volume using the Statistical Parametric Mapping software package (SPM8) (Ashburner and Friston, 2005), and following segmentation of the brain into tissue classes, only voxels with a probability higher than 98% of belonging to either WM, GM or CSF were kept (Keil et al., 2012).

2.4. Non-linear registration of anatomical images

Prior to the registration of T_1-weighted MPRAGE images to the MNI domain using the non-linear method, T_1-weighted MPRAGE images of

Table 1
A detailed description of the sequences and acquisition parameters for the estimation of water content using an intermediate TR method (Method A) and long TR method (Method B).

MPRAGE	a high-resolution T_1-weighted image (1 mm isotropic) was acquired using a magnetisation-prepared rapid gradient-echo sequence (MPRAGE) with TR = 2250ms, TE = 3.37ms, TI = 1100ms, FA = 15°, FOV = 256mm, 256×256 matrix, 176 sagittal slices, slice thickness = 1 mm, in an acquisition time of 9 min.
Method A	A 2D gradient-echo (GRE) sequence (PD-weighted) acquired with TR = 1.8s, TE = 5.8ms, FA = 40°, BW/pixel = 210Hz. The field-of-view (FOV) in-plane was 256×200mm^2 with 1mm in-plane resolution and 2mm slice thickness. Parallel imaging was employed with the generalised auto-calibrating partially parallel acquisition (GRAPPA) technique with an acceleration factor of 2 and 24 auto-calibration lines to acquire 64 transverse slices, read in two interleaved concatenations (resulting in a gap-free acquisition). The acquisition time was 6 min. For T_1 mapping, a T_1-weighted GRE scan acquired with TR = 500ms, TE = 5.8ms, FA = 90°, BW/pixel = 210Hz was used to acquire 64 transverse slices of 1mm in 1.7 min. The FOV in-plane was 256×200mm with 1mm in-plane resolution and 2 mm thickness. For $T_2{}^*$ mapping, an RF-spoiled multi-echo 3D-GRE MR acquisition with TR = 35ms, FA = 12°, BW/pixel = 510 Hz, TE1 = 2.3ms, ΔTE = 2.3ms, 8 echoes (3.4 min of acquisition time) with 1mm in-plane (2mm slice-thickness) was acquired to sample the decay of the recalled gradient echo as TE increases. For $B_1{}^+$ mapping four single-shot GRE-EPI scans (TE = 11ms, BW/ pixel = 2520Hz and FA = 30°, 60°, 90°, 120°), 2mm slice thickness, 2mm slice gap, image matrix 64×50, image FOV 256×200mm, 32 transverse slices where each volume acquisition was separated by 20s. The acquisition time was 1.2 min. For $B_1{}^-$ mapping, a set of two low-resolution GRE scans (TR = 500ms, TE = 5.8ms, BW/pixel = 210Hz and FA = 40°), in-plane resolution 4 mm, 32 transverse slices, slice thickness 2mm, slice gap 2mm were performed where the body coil was used in the place of the receive head array for signal reception in the second acquisition. The acquisition time was 1 min. The total acquisition time for Method A was TA = 13.5 min.
Method B	A 2D multiple-echo gradient-echo sequence acquired with TR = 10s and nominal flip angle of 90°. Other parameters were: FOV = 200×162mm; slice thickness = 1.50mm; 1.04 mm in-plane resolution; 1 mm slice gap; matrix size 192×117; 57 slices; phase resolution = 75%; bandwidth 280Hz/px; TE1 = 3.87ms; echo separation (ΔTE) 4.08ms, 12 echoes; and acceleration factor for parallel imaging (iPAT) 2. The acquisition time was 7.5 min. Indeed, in the interest of measurement time, the acquired phase resolution in Method B was chosen to be 75% of the nominal one. The images, however, are output at the nominal resolution, with interpolation being performed by the scanner software. This leads to the apparent inconsistency – the acquired in-plane resolution is 1.04×1.38 mm, and the in-plane resolution of the interpolated images is (1.04 mm)^2.

all subjects were aligned to the AC-PC line to help minimise registration errors, and all non-brain tissue was removed from every T_1-weighted MPRAGE volume using BET (Smith, 2002) (Brain Extraction Tool from FSL package).

The registration process was performed using the T_1-weighted MPRAGE volume as an input image and the common T_1-weighted MNI template as the reference image (avg152T_1_Brain template available in FSL package) for each subject.

The registration process of T_1-weighted MPRAGE to the MNI domain acquired from a representative subject is illustrated in Figure 3. Figure 3a shows an aligned transverse slice of the T_1-weighted MPRAGE scan and constitutes the input registered to the corresponding slice from the MNI template (3b) using the "3dwarper" program, which is part of the Automatic Registration Toolbox (ART) (http://www.nitrc.org/projects/art) (Ardekani et al., 2005). ART uses a free-form deformation based on cubic splines to perform the non-linear registration task. The non-linear transformation grid obtained after the registration process is shown in 3c, and 3d is the brain slice registered to the MNI template. The non-linear transformation matrix (3c) is further applied to the free water content map (3e) (and other imaging modalities; in figure T_1 map) to obtain free water content in the MNI domain (3f).

2.5. Linear registration of quantitative maps

Before creating the corresponding atlases for both methods, the acquired intra-subject quantitative water content maps were registered to subject-specific T_1-weighted MPRAGE using FSL-FLIRT (http://www.fmrib.ox.ac.uk/fsl) with 12-parameter affine transformation (Collins, 1995; Jenkinson and Smith, 2001). Thereafter, all measurements were registered to a common MNI template by applying the non-linear registration transformation obtained from the non-linear registration of the T_1-weighted MPRAGE scan to the MNI template.

2.6. Atlas generation

A schematic diagram for the generation of a quantitative water content brain atlas in MNI space coordinates is shown in Figure 4. The normalised water content maps were further used for atlas generation in the following way. Voxel-wise mean value, standard deviation and coefficient of variation (CoV = standard deviation/mean value) over all subjects were calculated using normalised water content maps. CoV describes the extent of variability in relation to the mean of the population. The final result is a 1 mm isotropic water content atlas, the standard deviation and coefficient of variation. Since one of the aims of this work was to assess possible method-related differences in building the atlas, we built a separate atlas for each method and refer in the following to $FW^{(\text{Method A})}$ and $FW^{(\text{Method B})}$ as atlases resulting from the corresponding methods (A and B, respectively).

2.7. Atlas analysis

In order to characterise different structures in the brain, twenty predefined regions-of-interest were assessed using the MNI structural atlas (Collins et al., 1994) and the Harvard-Oxford cortical and subcortical structural atlas (Desikan et al., 2006; Frazier et al., 2005; Goldstein et al.,

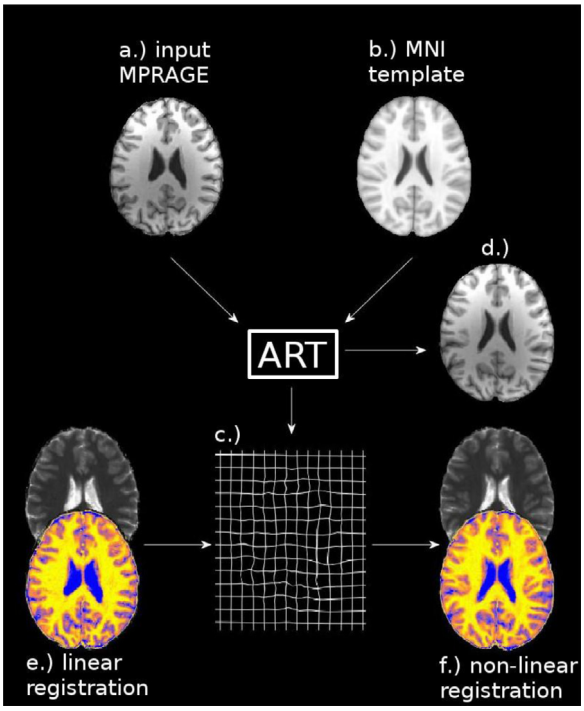

Figure 3. A representative illustration of the registration process is shown; a) is a transverse slice of the representative, input T_1-weighted MPRAGE, b) is the aligned slice from the MNI template, c) displays the non-linear transformation grid after registration from a representative subject, d) shows the registered slice of the brain to the MNI template, e) input free water content map and T_1 map which have been linearly co-registered with a) to take account of, for example, missing slices, f) registered slice of structural image and free water content map to the MNI template.

2007; Makris et al., 2006) listed in Table 2. Moreover, to estimate the free water content values for global white matter, grey matter and for cerebrospinal fluid separately, both atlases were segmented using SPM8. To efficiently suppress the influence of partial volume effects, all voxels, with WM, GM and CSF probabilities smaller than 98%, were set to zero (Keil et al., 2012).

2.8. Patient data analysis

The water content maps from a multiple sclerosis patient were acquired using Method A, and Method B was used to acquire the water content maps from a glioblastoma patient and a stroke patient. To ensure the validity of the comparison, these water content maps underwent the same processing pipeline (i.e., non-linear registration of quantitative water content maps) as the data from healthy control.

The water content maps were segmented into grey and white matter, as well as cerebrospinal fluid, using SPM8 segmentation. Voxel-wise z-score maps were calculated using z-score = ($FW^{Patient}$ - FW^{Atlas}) / Standard deviation FW^{Atlas}, and the differences between the patients' water content maps and the free water content atlases were further analysed using z-score maps.

The subject-specific CSF probability distributions can be obtained from the SPM-based segmentation of either the first GRE echo (Method B) or the water content maps (Method A). The tissue probability classes can be registered to the atlas using a registration transformation matrix (obtained from the registration of the anatomical images to a template) and can be compared to the z-score maps. The large differences in the probability for a given tissue class (CSF is the relevant one) can be interpreted as misregistration, and the z-score can be used for the detection of voxels with pathologically increased water content.

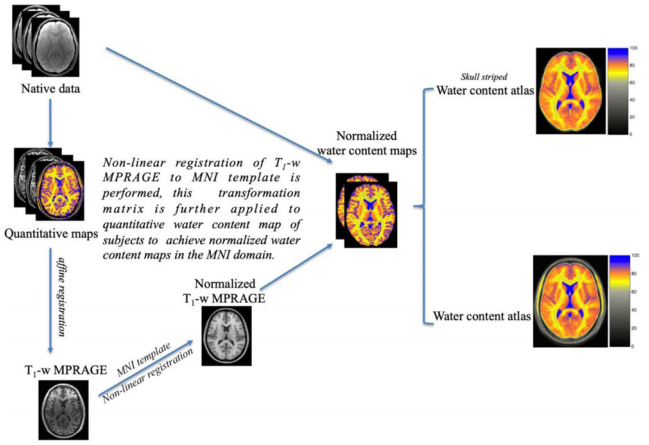

Figure 4. Pipeline demonstrating the steps involved for the generation of a quantitative water content brain atlas in MNI space coordinates. The water content maps were registered using linear registration to the T_1-w MPRAGE of every subject (i.e. intrasubject registration). In the second step, MPRAGE datasets were registered to the MNI template using *non-linear* registration. The same non-linear transformation was then used to register water content maps to the MNI template. Average water content was estimated for all subjects. This pipeline enables the acquisition and construction of an atlas with 1 mm isotropic resolution.

For each voxel included in the atlas, we have 20 independent measurements of its water content, and one can estimate the probability that the patient measurement is drawn from the same distribution. Within a normal distribution, for a given voxel in the patient's water content, if the z-score is three or higher, we concluded that the voxel has pathologically increased water content. Conversely, a negative z-score of three or lower in a given voxel was taken to indicate lower water content in the water content maps of patients.

3. Results

3.1. In vivo water content maps

Transverse slices of measured water content maps, obtained using both methods, from a representative participant are shown in Figure 5. Histograms of the whole-brain water content maps are displayed in the bottom row of Figure 5. Brain segmentation was performed, and the Gaussian fit over WM, GM and CSF regions is shown in the histogram. The average water content values for all volunteers, obtained from the entire WM and entire GM for Method A were 71.4(±4.4) and 81.3(±5.9). Comparatively, for Method B, the mean values of the Gaussian distributions of water content for the entire WM and entire GM were 70.8(±4.4) and 81.5(±5.5). These values show that despite the use of two different methods, the results for water content imaging are very similar in soft tissue, at least at the level of mean value per tissue class, and are in good agreement with the literature values at 1.5T and 3T (Abbas et al., 2014; Abbas et al., 2015; Gelman et al., 2001; Neeb et al., 2006b; Volz et al., 2012a; Warntjes et al., 2007a; Whittall et al., 1997) reported in Table 2.

3.2. In vivo water content atlas

Figure 6 displays axial slices of the two water content brain atlases acquired from the twenty healthy volunteers using Method A and Method B. The coefficient of variance and standard deviation using both methods are shown in Figures 6b and 6c.

The 2D histograms of the water content atlases estimated using Method A (*x*-axis) and Method B (*y*-axis) are shown in Figure 7. Qualitatively, the distribution appears to be well concentrated about the identity line.

Table 2
Water content atlas ($FW^{(\text{Method A})}$ and $FW^{(\text{Method B})}$) values and corresponding literature values in twenty regions-of-interest in the brain. Significant differences between the mean values in different ROI's are detected using Wilcoxon signed-rank test for p-value < 0.05 and are marked with an asterisk (*).

		Water content using atlases (percentage of pure water molarity)		
		This study		Literature (1.5T and 3T)
Brain regions		$FW^{(\text{Method A})}$	$FW^{(\text{Method 2})}$	
Cortical WM	**Frontal**	68.6±2.0	69.2±2.0	69.1±1.7(frontal)[3], 70.3±1.5[2], 70.8[4],
	Occipital	71.0±3.1	71.1±2.9	66.1±2.9 (frontal)[5], 68.4±1.9 (frontal),
	Parietal	70.1±1.4	70.4±1.7	72.7±2.1 (occipital), 70.3±1.3 (parietal),
	Temporal	72.0±3.0	69.9±2.7 *	72.5±1.3 (temporal)[6]
Cortical GM	**Frontal**	79.0±4.5	81.3±4.3	86.2±4.2 (prefrontal)[1], 81.6±1.6
	Occipital	79.2±4.7	78.7±4.9 *	(prefrontal)[3], 81.1±1.0[2], 83.2[4], 77.5±3.8
	Parietal	79.8±5.5	79.4±5.4 *	(frontal), 78.3±2.4 (occipital), 79.1±2.9
	Temporal	83.8±5.0	81.5±4.7 *	(parietal), 82.0±3.1 (temporal)[6]
Medulla		75.7±2.4	71.4±2.7 *	76.0±1.5[6]
Pons		73.3±2.8	73.4±3.1	73.2±2.4[6]
Midbrain		73.2±1.9	70.5±2.2 *	74.2±1.8[6]
Corpus Callosum	**Genu**	68.4±3.4	70.2±3.2	70.1±1.2[2], 71.7±1.0[4], 72.1±2.9[5], 69.6±4.6[6]
	Splenium	71.5±3.4	68.7±3.5 *	69.6±1.3[2], 70.5±4.7[6]
Caudate (head)		82.4±1.6	83.7±2.0	81.1±2.5[1], 81.5±1.0[2], 84.8±1.7[3], 81.3±2.2[5], 83.0±1.3[6]
Globus Pallidus		76.4±2.1	74.4±2.6 *	76.8±1.9[6]
Putamen		81.6±1.7	82.3±1.9	81.9±1.1[2], 83.2±1.6[3], 83.1±0.9[4], 82.3±2.6[5], 81.9±1.3[6]
Hippocampus		80.9±3.0	82.9±2.7	82.0±1.9[6]
Thalamus		81.6±1.6	79.5±1.9 *	73.4±3.4[1], 79.8±1.0[4], 81.0±2.2[5], 82.5±1.7[6]
Insula		81.4±2.2	81.8±2.2	82.9±1.4[6]
Anterior lateral ventricle		99.0±4.7	95.7±4.5 *	99.9±3.7[6], 100 (expected)
(1) (Gelman et al., 2001)				(4) (Whittall et al., 1997)
(2) (Volz et al., 2012b)				(5) (Warntjes et al., 2007b)
(3) (Neeb et al., 2006b)				(6) (Abbas et al., 2015)

Furthermore, we performed segmentation of the water content atlases. The water content values from water content atlases using Method A and Method B were 71.1 (±2.8) and 70.5(±2.9) for WM, and 81.4(±4.4) and 81.7(±4.2) for GM, respectively.

Further comparisons between the water content values from both atlases were made using twenty regions-of-interest containing soft tissue and regions of cerebrospinal fluid. There were no statistically significant mean value differences between the left and the right cerebral hemispheres. Therefore, pooled data (from the left and right hemispheres) were used for statistical analysis. The mean values from "Method A" ($FW^{(\text{Method A})}$) and "Method B" ($FW^{(\text{Method B})}$) and standard deviations over all volunteers are reported in Table 2.

Significant differences between the mean values in different ROIs were assessed using the Wilcoxon signed-rank test for p-value < 0.05 and are marked with an asterisk (*) in Table 2.

The mean water content atlas values in most of the WM and GM ROIs are in good agreement and are also in agreement with the literature values reported previously. However, some WM and GM structures, namely the medulla, midbrain, splenium of the corpus callosum, and thalamus, showed significant differences between the values assessed using both methods.

3.3. Water content atlas comparison to patient data

Water content maps generated from a glioblastoma tumour patient and a stroke patient using Method B and registered to the water content atlas using linear and non-linear registration were compared to the water content atlas obtained from the healthy volunteers using Method B and are shown in Figure 8 for the glioblastoma patient and in Figure 9 for the stroke patient. Both figures are subdivided into two rows, and the results from linear and non-linear registration are shown in the top and bottom rows, respectively. Comparison between the patient data and the atlases generated using Methods A and B are shown in Supplementary Materials 1.

Figure 8a shows a transverse slice from the water content atlas, and the corresponding slice of the free water content map (after linear registration to the water content atlas) from the glioblastoma patient is shown in 8b. The absolute differences between the water content atlas and the water content map from the patient for a slice containing the brain tumour are shown in Figure 8c. Figure 8d shows the region of the 'significant difference' z-score (corresponding to z-score>3 and z-score <-3) overlaid on a structural image. Figure 8e shows a slice of the FLAIR image for the same patient. Figures 8f to 8j in the bottom row show the same analysis, but with the map of the glioblastoma patient registered to the water content atlas using non-linear registration. The regions of 'significant differences' obtained after either linear or non-linear registration highlight very similarly affected regions.

Figure 9a shows a transverse slice from the water content atlas, and the corresponding slice of the free water content map from a stroke patient (Figure 9b). The absolute differences between the water content atlas and the water content map from the stroke patient for a slice containing oedema are shown in Figure 9c. Figure 9d shows the region of the 'significant difference' z-score (corresponding to z-score>3 and z-score <-3) was overlaid on a structural image. Figure 9e shows a slice of the FLAIR image for the same patient. Figures 9f to 9j in the bottom row show the same analysis, but with the map of the stroke patient co-registered to the water content atlas using non-linear registration. The regions of 'significant difference' z-score matches well with the oedema region present in the FLAIR image.

To further evaluate the usefulness of the water content atlases, the water content map acquired from a MS patient – using Method A – was compared to the water content atlas obtained from the healthy volunteers also using Method A. The absolute differences between the water content map of an MS patient and the water content atlas are shown in Figure 10c. The region of the 'significant difference' z-score is shown in Figure 10d and MPRAGE image for the same patient is shown in Figure 10e. Figures 10f to 10j in the bottom row show the same analysis, but with the map of the MS patient registered to the water content atlas using non-linear registration.

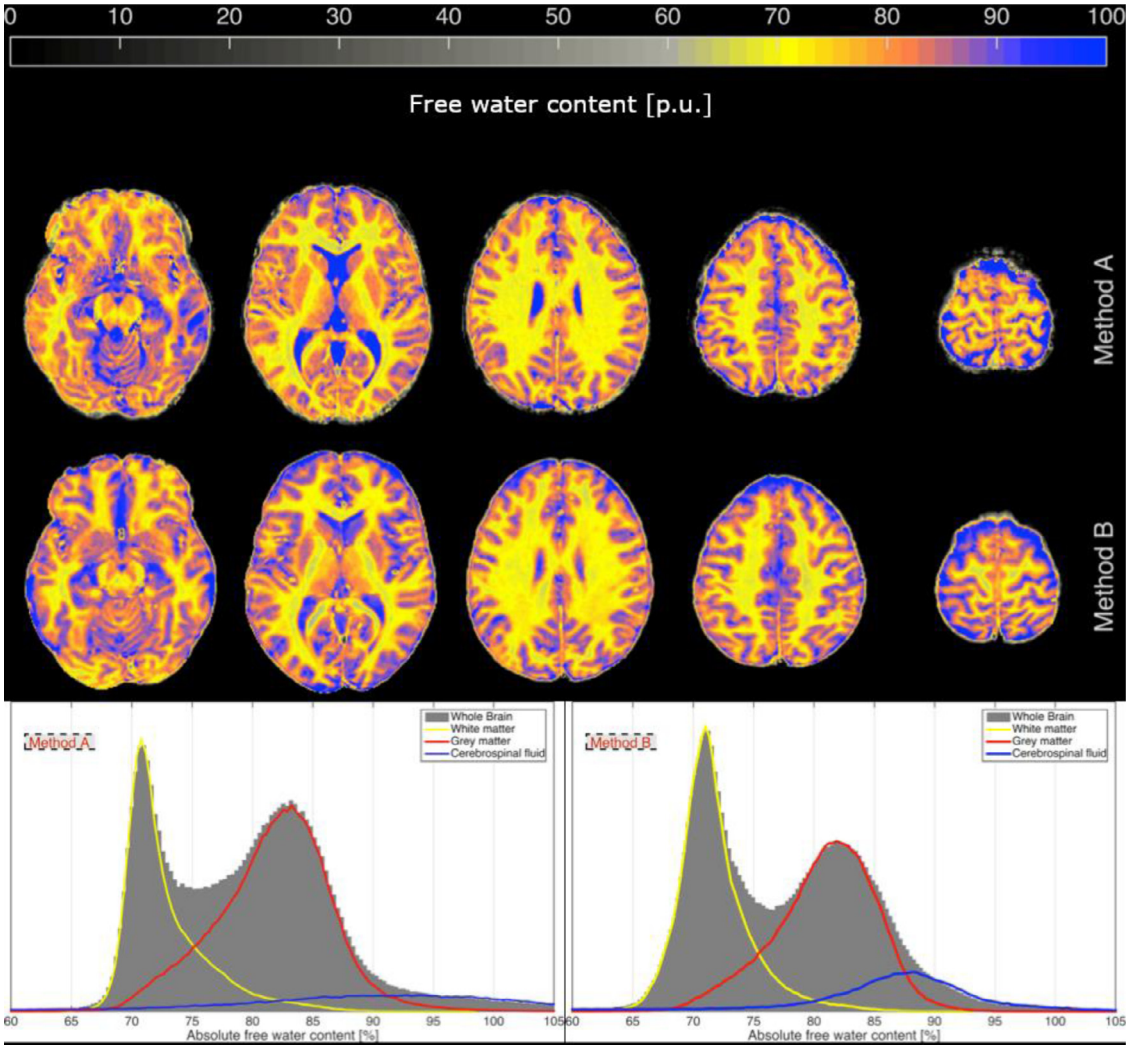

Figure 5. Quantitative measure of the water content from a representative healthy participant using Method A and Method B. Histograms values of the water content in percent for segmented white matter, grey matter and cerebrospinal fluid are shown.

4. Discussion

In this work, previously validated experimental protocols for water content mapping were used to gather quantitative data sets from twenty healthy volunteers. The acquired data enabled the derivation of quantitative water content maps with full brain coverage. Furthermore, this work represents the development of the first quantitative *in vivo* water content brain atlas in the MNI domain. By using a nonlinear registration approach for image registration, the effect of brain size and intra-subject cortical variations was minimised, giving it an added advantage compared to the linear registration method. It also helped to minimise the standard deviation of water content and supported a reduction in potentially systematic errors. The final water content atlas is presented in the MNI coordinate system and can be easily converted to other coordinate systems, e.g., ICBM, making it practicable and easily accessible for the scientific community and clinicians.

The water content brain atlas was further exploited by choosing different soft tissue ROIs, which were evaluated and analysed in order to investigate possible differences between two commonly used water mapping methods; statistical analysis was performed to assess significant differences.

The atlases generated by both experimental methods were used to investigate systematic differences between them and individual input water maps (e.g. from patients) as no 'gold-standard' for a quantitative water content atlas currently exists. A reliable and reproducible atlas requires systematic fluctuations of the originally measured water content for each subject to be as small as possible. Statistical fluctuations are also important and should be minimised, although their influence on the result is probably not as relevant as that of systematic effects. Statistical fluctuations can be kept in check by increasing the number of subjects contributing to the atlas. However, if many specialised atlases are to be created, such as age- and gender-specific atlases, the number of volunteers contributing to each atlas is typically limited since logistical and organisational constraints also need to be considered. Moreover, especially for the older population, it is increasingly difficult to find healthy volunteers who meet all inclusion criteria (see, for example, (Mazziotta et al., 2009)).

An important motivation behind the development of a quantitative water content atlas is its use as a sensitive reference tool for the detection of diseases inducing a pathological change in brain tissue water content. Indeed, comparison to the atlas makes the comparison to the contralateral region (which could also be affected, depending on pathology, medication, etc.) superfluous and eliminates an important subjective aspect in reporting changes in water content. Therefore, it is very important to include possible physiological variations of the water content in a healthy population, such as dehydration, while specifically excluding pathological processes, which might modify the brain water content. That said, in accordance with previous, unpublished experiments

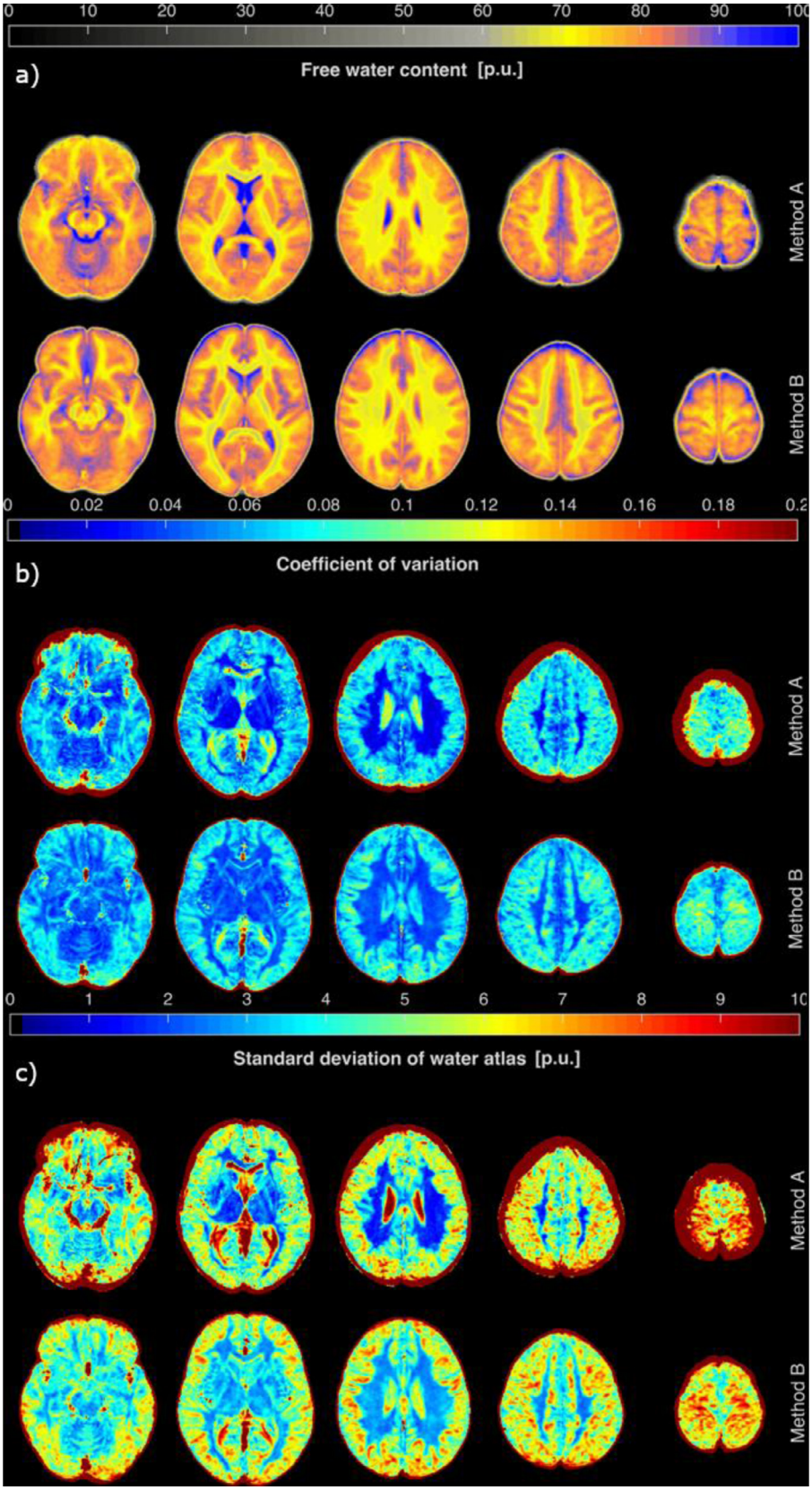

Figure 6. Axial slices of water content brain atlases acquired from twenty right-handed healthy male participants aged (25.3 ± 2.5) using Method A and Method B. The coefficient of variance and standard deviation using both methods are shown in 6b (middle row) and 6c (bottom row). Note that the coefficient of variance of 0.1 refers to a relative deviation of 10% in the water content.

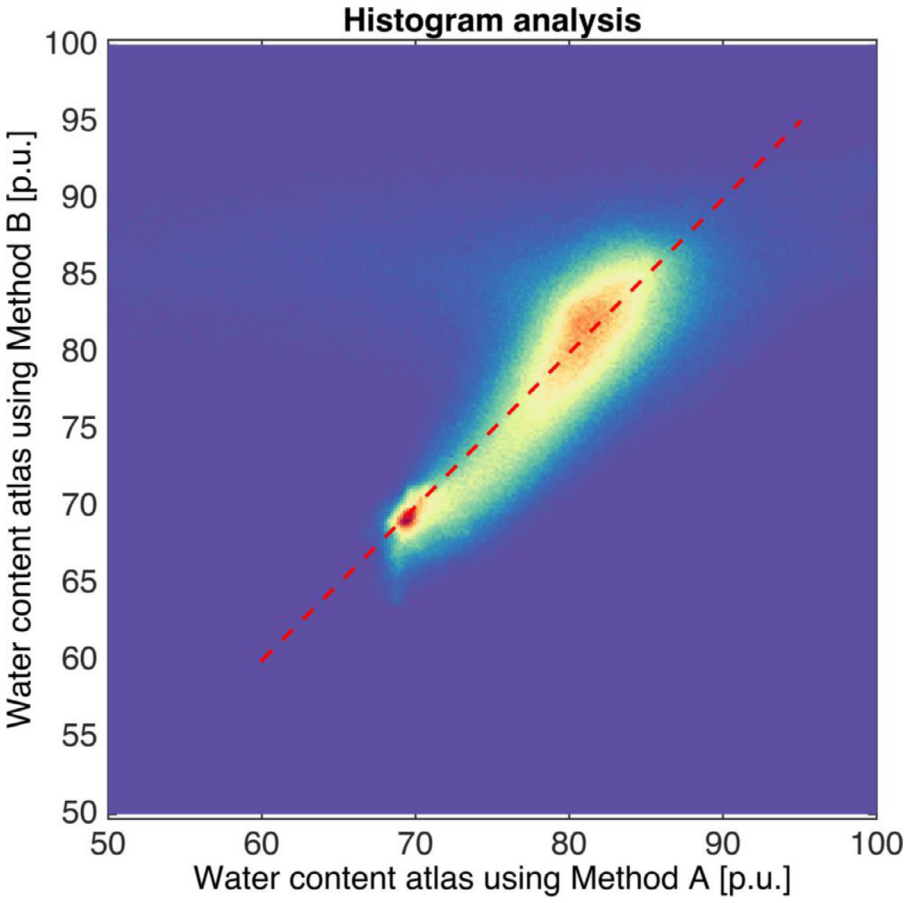

Figure 7. 2D-histogram analysis of water content atlases obtained using Method A (x-axis) and Method B (y-axis). Clustering around the identity line shows good agreement between the two methods.

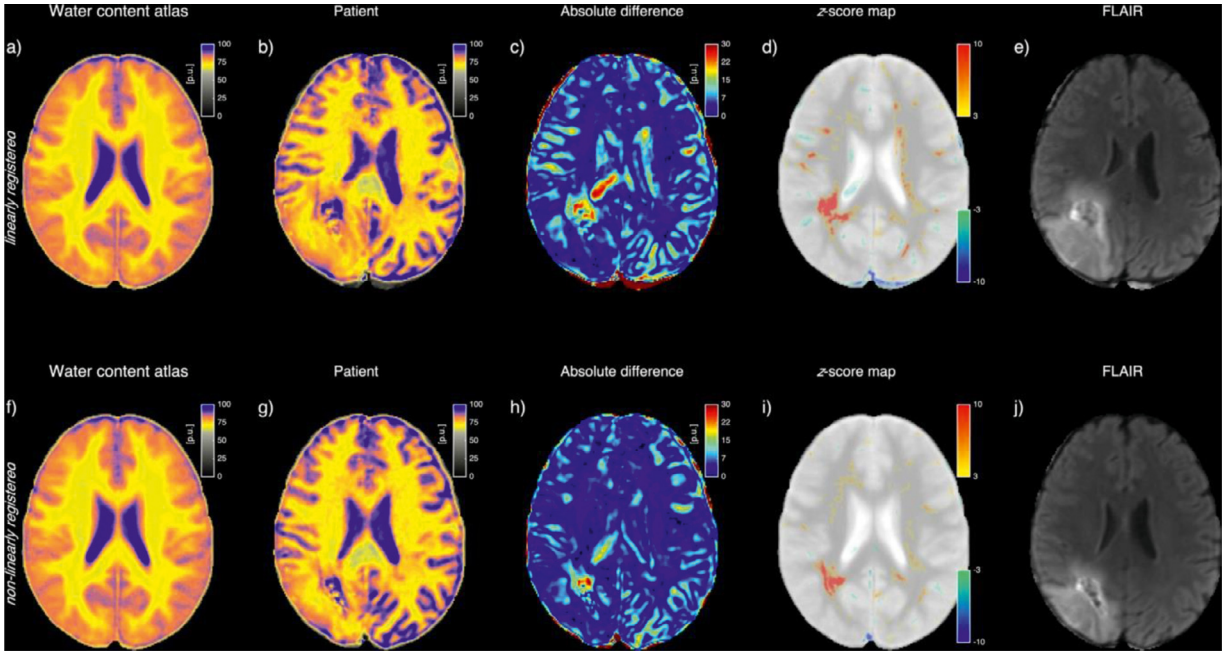

Figure 8. Influence of linear versus non-linear registration of atlas images acquired using Method B. Top row: (a) axial slice of a water content atlas (Method B) and (b) a free water content map from the glioblastoma tumour patient co-registered to (a) using *linear* registration, (c) along with the absolute differences between the map and the atlas and (d) an estimation of brain oedema using a z-score (an overlaid map). Bottom row: Figures 8f to 8j show the same analysis between the water content atlas acquired using Method B and a free water content map for the same glioblastoma patient co-registered to (a) using *non-linear* registration.

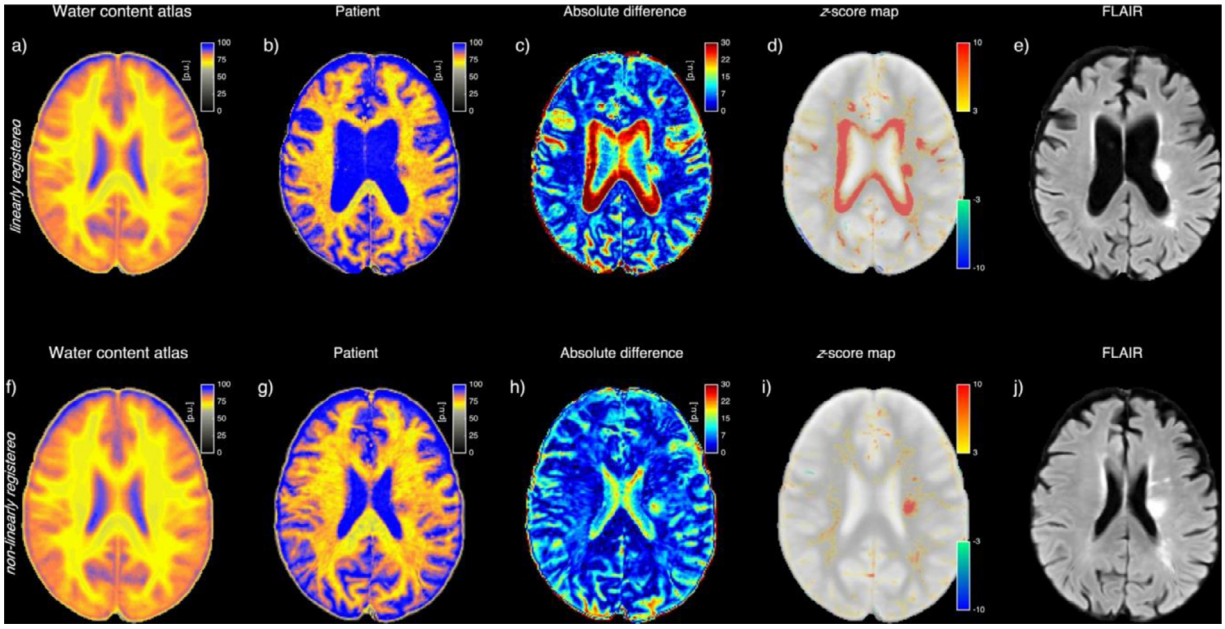

Figure 9. Influence of linear versus non-linear registration of atlas images acquired using Method B. Top row: (a) axial slice of a water content atlas (Method B) and (b) a free water content map from the stroke patient co-registered to (a) using linear registration, (c) along with the absolute differences between both maps and (d) an estimation of brain oedema using a z-score (an overlaid map). Bottom row: Figures 9f to 9j show the same analysis between the water content atlas acquired using Method B and a free water content map for the same stroke patient co-registered to (a) using non-linear registration. Note, in the bottom row, although non-linear registration has been used to co-register a) and b), it is shown that type of registration only affects ventricles and *not* the stroke region.

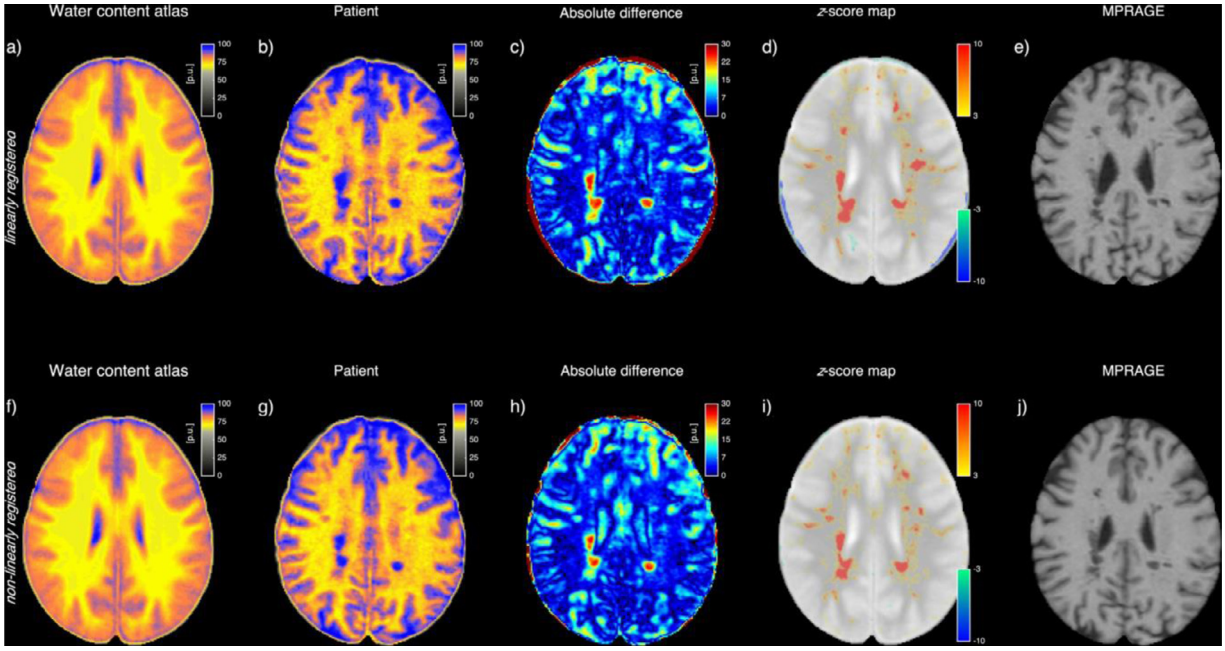

Figure 10. Influence of linear versus non-linear registration of atlas images acquired using Method A. Top row: (a) axial slice of a water content atlas (Method A) and (b) a free water content map from the multiple sclerosis patient co-registered using linear registration, (c) along with the absolute differences between both maps and (d) an estimation of brain oedema using a z-score (an overlaid map). Bottom row: Figures 10f to 10j show the same analysis between the water content atlas acquired using Method A and a and free water content map for the same multiple sclerosis patient co-registered using non-linear registration. Note, in the bottom row, although non-linear registration has been used to co-register a) and b), it is shown that type of registration only affects ventricles and *not* the multiple sclerosis lesion.

carried out in-house to investigate the possible influence of hydration status on the brain water content, it was not regarded as necessary to explicitly check the individual hydration status of the volunteers. This is because the blood-brain barrier is known to keep the brain water content constant, even after exhaustive sporting exercise or dehydration (Maughan et al., 2007). In this regard, several studies (Duning et al., 2005; Kempton et al., 2007; Meyers et al., 2016) have tried to investigate the effect of controlled dehydration and rehydration on the brain volume using MRI and voxel-wise analysis such as SIENA (Structural Image Evaluation, using Normalization, of Atrophy) in the FSL package. The volumetric changes reported were below 1% for dehydration as well as for rehydration (Duning et al., 2005). Kempton et al. (Kempton et al.,

2007) did not report any change in the total brain volume but an increase in the ventricular volume in some of the volunteers. However, none of these studies were performed using a quantitative measurement technique to specifically measure water content.

The goal of using two different approaches for the generation of a water content atlas was: (1) to investigate how many subjects are necessary to form an optimised water content atlas; see Supplementary Materials 3; and (2) identify which approach minimised statistical and potentially systematic errors; see Supplementary Materials 2; and whether different methods give rise to similar quantitative water content atlases. This would allow the future inclusion of water content maps acquired using different available techniques. However, due to the lack of a 'gold-standard' method of localised brain water content *in vivo*, it is not obvious how to define characteristic parameters in order to identify the most stable and reliable result. In the current work, the voxel-wise standard deviation and the coefficient of variation of the water content distribution were calculated. The corresponding maps provide information about the reliability of the method. In this case, higher CoV values were found in CSF, which is in line with the previous reports due to higher T_1 values of CSF and/or motion of CSF. The use of a CoV map together with a water content atlas could be useful to detect and analyse pathologies as it defines the extent of variability in relation to the mean of the population, i.e., removal of outliers from the analysis.

The average values for both approaches evaluated here did not differ significantly in global WM, global GM and in lobe-wise WM and GM structures. However, in sub ROI analysis, we found significant differences in the medulla, midbrain and in the thalamus using the Wilcoxon signed-rank test. Nevertheless, the average values lie within a single standard deviation. We mention that the CSF 'water content' obtained by Method B includes a T_1 saturation factor. Indeed, for a T_1(CSF) of 4.3 s at body temperature (Rooney et al., 2007), and using a 90-degree flip angle for maximum SNR, not even a TR of 10s can prevent remnant steady-state effects in CSF. In contrast, Method A provides a measure for T_1 of CSF, although considerably longer than the T_1 interval for which the two-point method was optimised. The CSF water content obtained by Method A should, thus, ideally be 100%. Differences from this value reflect the mentioned suboptimal fitting of CSF properties when the accuracy of the two-point method is optimised for tissue properties. The application of the atlases generated using Methods A and B to examine changes in a glioblastoma patient and a stroke patient showed very similar pathologies, i.e., inter-method regions similar to intra-method regions were detected – marked as voxels with z-score (z-score of three or higher is predominantly indicative of voxels with increased water content); see Supplementary Materials 1. This affirms the stability of the water content atlas and could enable the use of either Method A or Method B to acquire water content maps for comparison with the atlas.

It is explicitly noted that the ages of the patients reported here differed markedly from the mean age of the healthy subjects comprising the atlases. Two approaches could be followed to mitigate this confound: (a) generate age-specific atlases and use those for comparison; or (b) given that the age dependence of water content in the brain has been previously reported (Neeb et al., 2006a), a simple scaling factor (separately for GM and WM) could be applied prior to statistical analysis.

As an indication of the usefulness of the atlas-based approach, here we report on an objective way of detecting oedema, as a significant increase in water content in the patient's brain compared to the atlas. It was possible to detect relatively small regional water content changes (starting from 3pu) in stroke, highlighting the precision of the water content mapping methods used both in the clinical context, and for generating the atlases.

The standard deviation of the atlas-based water content in WM of around 3pu (or 0.04 CoV) allows the detection of a water content increase of around twice this value at the voxel level. This is a very substantial change of 5-6pu, and many pathologies (such as acute stroke or inflammation) are known to produce smaller changes. The sensitivity of detection is, however, substantially higher for an ROI-based comparison. Depending on the clinical question and on the availability of other contrasts with which to define a conspicuous ROI, the comparison with the atlas can be performed either on a voxel-based or an ROI-based level. In order to address the significance of water content changes for an ROI-based comparison, we would recommend a simple Monte-Carlo simulation along the following lines. In every voxel of the ROI, a Gaussian distribution characterised by the mean and standard deviation in the voxel, according to the atlas, would be used to draw values. This should be repeated many times, and the mean water content and standard deviation for the ROI would be thus calculated. The values based on the atlas data should then be compared to the experimental values and the significance of changes assessed using common statistical tests. The same is valid for ROIs containing GM, where the standard deviation is even higher due to imperfections of the registration and partial voluming with CSF.

In summary, we have developed and introduced the first quantitative water content brain atlas *in vivo*. Both experimental approaches studied here to acquire the underlying data provide stable and reliable results, representing the average water content of a healthy population and a certain inter-subject anatomical variability based on MNI coordinates. Both atlases provide similar water content values as proven using ROIs analysis. This strongly encourages one to use any of these defined methods for water content imaging in healthy volunteers and to generate further water content atlases based on age and gender.

Since the calculation of water content maps is based on the determination of quantitative T_1 (in intermediate TR method) and T_2^* maps, quantitative T_1 and/or T_2^* maps are a prerequisite for water content mapping. This means that T_1 and T_2^* atlases could, additionally, be produced to provide further supplementary information. Thus, all three atlases form a solid basis for further development, especially for the investigation of diseases such as multiple sclerosis or hepatic encephalopathy, which show pathological changes in relaxation times and/or tissue water content (Shah et al., 2008). The combination of atlas-based features of water content, T_1 and T_2^* mapping with clinical information has the potential to form the basis for a multidimensional analysis of characteristic disease properties, which could allow for a much more individualised diagnosis and the prediction of future disease burden. To realise this, well-organised and large multi-centre studies with large patient populations are necessary.

5. Conclusion

In summary, the current work demonstrates the development of the first quantitative *in vivo* water content brain atlas at 3T, representing the average water content of 20 healthy volunteers in MNI space. Two methods were investigated for the acquisition of the water content maps, demonstrating the generality of the atlas. A preliminary investigation of patient data hints towards the potential importance of atlases in clinical applications, however, to the best of our knowledge, no comprehensive studies on the application of water content atlases in patient cohorts have been conducted, and the relevance of water content atlases remains a moot point.

For future work, it would be straightforward to produce additional T_1 and T_2^* relaxation time atlases enabling 'multi-modal' characterisation of, for example, the inflammatory component of brain diseases. This further development can potentially shed light on patient cohorts such as those with traumatic brain injury, idiopathic normal pressure hydrocephalus etc., where pathological changes are reflected by variations in relaxation times and/or tissue water content.

Data and Code Availability Statement

All relevant data are within the paper and its Supporting Information files. Nevertheless, the correspondence author N. J. Shah can be contacted at n.j.shah@fz-juelich.de for further questions.

Supplementary materials

Supplementary material associated with this article can be found, in the online version, at doi:10.1016/j.neuroimage.2022.119014.

Appendix A

In order to demonstrate the generality of the water content atlas, two prominent methods for data acquisition were compared.

Method A

Quantitative water content was calculated by applying the following transformations to the PD-weighted scan: i) compensation for the transmit (B_1^+) and receive field (B_1^-) inhomogeneity ii) compensation of the T_2^* decay and iii) correction of the T_1-saturation effect by obtaining the T_1 relaxation time using the so-called two-point technique (Deoni et al., 2003; Parker et al., 2001).

The B_1^+ distribution was measured using the multiple FA (MFA) technique (Hornak et al., 1988; Weber et al., 2010). This uses a series of four single-shot GRE-EPI scans with the scan parameters described in Table 1. Each acquisition volume was separated by 20 seconds to ensure full relaxation of the magnetisation, i.e., TR > $5T_1$; at 3T WM is ~ 1s, GM is ~ 1.5s, and cerebrospinal fluid is ~ 4s. These four low-resolution EPI images were used to calculate the actual FA distribution.

Estimation of the receiver profile (i.e. B_1^- distribution) was achieved using a set of two low-resolution GRE scans with the scan parameters described in Table 1. Here, the second scan was acquired using the body coil for signal reception instead of the receive head array (Abbas et al., 2014; Neeb and Shah, 2006).

An acquisition using an RF-spoiled multi-slice, multi-echo GRE sequence was performed to sample the echo decay as a function of TE. Assuming an exponential decay, this dataset enabled calculation of the T_2^* decay constant and a subsequent correction of T_2^* decay present in the PD-weighted scan. The sequences for mapping T_1, T_2^*, B_1^+ and B_1^- were adjusted to the same slice orientation and FOV as the PD-weighted scan. The total scan time for the water mapping protocol was 13.5 min.

RF bias correction and image normalisation

Following the application of the corrections for T_1, T_2^*, B_1^+ and B_1^- to the PD-weighted data, the resulting dataset, S_0, represents the MR-visible water content map. However, it has already been reported that the receiver profile estimation, B_1^-, is biased if the transmit and receive profiles of the body coil, $B_1^{+(BC)}$=B_1^+ and $B_1^{-(BC)}$, differ (Abbas et al., 2014; Abbas et al., 2015; Oros-Peusquens et al., 2014) and this gives rise to a multiplicative bias, $b = B_1^{+(BC)} / B_1^{-(BC)}$. This effect is unfortunately compounded at 3 T.

For the compensation of RF bias, a recently proposed method (Abbas et al., 2014) for 3 T was used. The RF bias was estimated by exploiting the well-known correlation between the T_1 relaxation time and water content (Abbas et al., 2014). This technique assumes a deterministic linear relationship between $1/T_1$ and 1/PD (Fatouros et al., 1991; Volz et al., 2012a) within a region of the brain satisfying the condition of T_2^* > 50ms and T_2^* < 60ms (Abbas et al., 2014).

By normalising this image—referred to as the non-calibrated PD image—to the ventricular cerebrospinal fluid (CSF) signal, the water molarity of the tissue is obtained as a percentage of the CSF water content, which is very close to that of pure water. For this normalisation, a recently proposed approach (Abbas et al., 2014; Abbas et al., 2015) was used where CSF signal (S_0^{CSF}) is estimated as follows:

i) the entire right and left ventricles are segmented using a semi-automated approach. First, gross localisation is performed by enclosing the ventricle in an ellipsoid, and this is followed by segmentation - within the ellipsoid, based on T_1 and T_2^*: r ∈ left or right ventricle if T_1 > 2900ms and T_2^* > 500ms.
ii) The segmented region, denoted by V, is partitioned into sub-regions $(Vi)_{0<i<n}$ of constant B_1^{Tx} values (practically $\Delta B_1^{Tx}/B_1^{Tx} < 1$).
iii) Within each iso-B_1^{Tx} region, V_i, the average of PD-weighted and the T_1-weighted GRE signals (corrected against receiver profile inhomogeneity) - $S_{PD\text{-}w,i}$ and $S_{T1\text{-}w,i}$ are computed.
iv) Assuming that these signals obey the Ernst equation (in V_i the FA is constant), the underlying parameters $S_{0,i}^{(CSF)}$ and $T_{1,i}^{(CSF)}$ are subsequently estimated as described above.
v) The final CSF signal is computed from the weighted average $S_0^{CSF} \equiv S\ |V|^{-1}\ \Sigma_{i=1}^{n} |V_i| S_{0,i}^{CSF}$, where $|V|$ denotes the number of voxels contained in V. Averaging the GRE signals allows minimisation of the effect of noise on the normalisation of the PD image to the water signal (Abbas et al., 2014; Abbas et al., 2015). The weighted average S_0^{CSF} is used for the water content calibration.

Method B

Magnitude and phase data were saved for each echo and processed offline. A mono-exponential fit to the signal decay as a function of echo time delivered the effective transverse relaxation time (T_2^*) and signal intensity at TE = 0 ms. In order to relate the signal intensity at TE = 0ms to water content, two additional steps were required:(a) correction for transmit and receive inhomogeneities and (b) calibration to a reference with known water content. Since all corrections are multiplicative in this long TR method, step (a) was performed using a bias field correction as implemented, for example, in SPM (Ashburner and Friston, 2005) and step (b) by calibrating to the CSF signal intensity, considered to represent 100% water. Due to the very long repetition time, T_1 saturation can be neglected for brain tissue at 3T.

The use of CSF water content as a calibration standard is very convenient since the region is already included in the brain, but not without problems. Instead of displaying a very sharp peak, as expected for a homogeneous compartment, the quantitative properties of CSF show a broad distribution. This is most likely due to the presence of pulsation. The mode of this distribution, however, was found to be very stable in Method B and corresponds to voxels from the lateral ventricles, which are were selected by a quantitative mask in Method A. The use of an external standard would not only complicate the measurements but also increase the variability of the calibration due to uncertainty in extrapolating the B_1^- distribution, which is derived – using SPM or T_1-water content correlations - for the brain region only.

However, the long T_1 value of CSF requires a small T_1 correction to the CSF signal intensity. Based on the measured effective flip angle in CSF and a T_1 value of 4.3 s (Rooney et al., 2007), a correction factor of 0.94 was calculated and used throughout.

References

Abbas, Z., Gras, V., Mollenhoff, K., Keil, F., Oros-Peusquens, A.M., Shah, N.J., 2014. Analysis of proton-density bias corrections based on T1 measurement for robust quantification of water content in the brain at 3 Tesla. Magn. Reson. Med. 72, 1735–1745.

Abbas, Z., Gras, V., Möllenhoff, K., Oros-Peusquens, A.-M., Shah, N.J., 2015. Quantitative water content mapping at clinically relevant field strengths: A comparative study at 1.5T and 3T. Neuroimage 106, 404–413.

Ardekani, B.A., Guckemus, S., Bachman, A., Hoptman, M.J., Wojtaszek, M., Nierenberg, J., 2005. Quantitative comparison of algorithms for inter-subject registration of 3D volumetric brain MRI scans. J Neurosci Methods 142, 67–76.

Ashburner, J., Friston, K.J., 2000. Voxel-based morphometry–the methods. Neuroimage 11, 805–821.

Ashburner, J., Friston, K.J., 2005. Unified segmentation. Neuroimage 26, 839–851.

E. M.; Bloembergen, N.P., Pound, R.V, 1948. Relaxation Effects in Nuclear Magnetic Resonance Absorption. Phys. Rev. 73, 679–712.

Broca, P., 1861. Perte de la parole: ramollissement chronique et destruction partielle du lobe anterieur gauche du cerveau. Bulletins de la Societe d'anthropologie 2, 235–238.

Brodmann, K., 1905. Beitraege zur histologischen Lokalisation der Grosshirnrinde: dritte Mitteilung: Die Rindenfelder der niederen Affen. Journal fuer Psychologie und Neurologie 4-5, 177–226.

Brodmann, K., 1909. Vergleichende Lokalisationlehre der Grosshirnrinde in ihren Prinzipien dargestellt auf Grund des Zellenbaues. Johann Ambrosius, Barth, Leipzig.

Collins, D.L., Neelin, P., Peters, T.M., Evans, A.C., 1994. Automatic 3D intersubject registration of MR volumetric data in standardized Talairach space. J Comput Assist Tomogr 18, 192–205.

C.; Collins, L.H., Peters, T., Evans, A, 1995. Automatic 3D Model-Based Neuroanatomical Segmentation. Hum. Brain Mapp. 3, 190–208.
Deoni, S.C., Rutt, B.K., Peters, T.M., 2003. Rapid combined T1 and T2 mapping using gradient recalled acquisition in the steady state. Magn. Reson. Med. 49, 515–526.
Draganski, B., Gaser, C., Busch, V., Schuierer, G., Bogdahn, U., May, A., 2004. Neuroplasticity: changes in grey matter induced by training. Nature 427, 311–312.
Duning, T., Kloska, S., Steinstrater, O., Kugel, H., Heindel, W., Knecht, S., 2005. Dehydration confounds the assessment of brain atrophy. Neurology 64, 548–550.
Evans, A.C., 1993. 3D statistical neuroanatomical models from 305 MRI volumes. Nuclear Science Symposium and Medical Imaging Conference 3, 1813–1817.
Fatouros, P.P., Marmarou, A., Kraft, K.A., Inao, S., Schwarz, F.P., 1991. In vivo brain water determination by T1 measurements: effect of total water content, hydration fraction, and field strength. Magn. Reson. Med. 17, 402–413.
Gaser, C., 2005. Morphometrie. Funktionelle Bildgebung in Psychiatrie und Physiotherapie. H. Walter, Stuttgart, pp. 89–104.
Gelman, N., Ewing, J.R., Gorell, J.M., Spickler, E.M., Solomon, E.G., 2001. Interregional variation of longitudinal relaxation rates in human brain at 3.0 T: relation to estimated iron and water contents. Magn. Reson. Med. 45, 71–79.
Good, C.D., Johnsrude, I.S., Ashburner, J., Henson, R.N., Friston, K.J., Frackowiak, R.S., 2001. A voxel-based morphometric study of ageing in 465 normal adult human brains. Neuroimage 14, 21–36.
Gras, V., Abbas, Z., Shah, N.J., 2013. Spoiled FLASH MRI with Slice Selective Excitation: Signal Equation with a Correction Term. Concepts in Magnetic Resonance Part A 42, 89–100.
Hornak, J.P., Szumowski, J., Bryant, R.G., 1988. Magnetic field mapping. Magn. Reson. Med. 6, 158–163.
Jenkinson, M., Smith, S., 2001. A global optimisation method for robust affine registration of brain images. Med Image Anal 5, 143–156.
Keil, F., Oros-Peusquens, A.M., Shah, N.J., 2012. Investigation of the spatial correlation in human white matter and the influence of age using 3-dimensional variography applied to MP-RAGE data. Neuroimage 63, 1374–1383.
Kempton, C.L., Soucie, J.M., Abshire, T.C., 2007. Incidence of inhibitors in a cohort of 838 males with hemophilia A previously treated with factor VIII concentrates (vol 4, pg 2576. 2006). J. Thromb. Haemost. 5, 657 -657.
Mandal, P.K., Mahajan, R., Dinov, I.D., 2012. Structural brain atlases: design, rationale, and applications in normal and pathological cohorts. J Alzheimers Dis 31 (Suppl 3), S169–S188.
Maughan, R.J., Shirreffs, S.M., Watson, P., 2007. Exercise, heat, hydration and the brain. J Am Coll Nutr 26, 604S–612S.
Mazziotta, J.C., Toga, A.W., Evans, A., Fox, P., Lancaster, J., 1995. A probabilistic atlas of the human brain: theory and rationale for its development. The International Consortium for Brain Mapping (ICBM). Neuroimage 2, 89–101.
Mazziotta, J.C., Woods, R., Iacoboni, M., Sicotte, N., Yaden, K., Tran, M., Bean, C., Kaplan, J., Toga, A.W.Members of the International Consortium for Brain, M., 2009. The myth of the normal, average human brain–the ICBM experience: (1) subject screening and eligibility. Neuroimage 44, 914–922.
Mechelli, A., Crinion, J.T., Noppeney, U., O'Doherty, J., Ashburner, J., Frackowiak, R.S., Price, C.J., 2004. Neurolinguistics: structural plasticity in the bilingual brain. Nature 431, 757.
Mechelli, A., Friston, K.J., Frackowiak, R.S., Price, C.J., 2005. Structural covariance in the human cortex. J Neurosci 25, 8303–8310.
Meyers, S.M., Tam, R., Lee, J.S., Kolind, S.H., Vavasour, I.M., Mackie, E., Zhao, Y.S., Laule, C., Madler, B., Li, D.K.B., MacKay, A.L., Traboulsee, A.L., 2016. Does hydration status affect MRI measures of brain volume or water content? J. Magn. Reson. Imaging 44, 296–304.
Neeb, H., Shah, N.J., 2006. Enhancing the precision of quantitative water content mapping by optimizing sequence parameters. Magn. Reson. Med. 56, 224–229.
Neeb, H., Zilles, K., Shah, N.J., 2006a. Fully-automated detection of cerebral water content changes: study of age- and gender-related H2O patterns with quantitative MRI. Neuroimage 29, 910–922.
Neeb, H., Zilles, K., Shah, N.J., 2006b. A new method for fast quantitative mapping of absolute water content in vivo. Neuroimage 31, 1156–1168.
T.; Neeb, H.D., Shah, N.J., 2004. Quantitative T1 mapping and absolute water content measurement using MRI. International Congress Series 1265, 113–123.
Oros-Peusquens, A.M., Keil, F., Langen, K.J., Herzog, H., Stoffels, G., Weiss, C., Shah, N.J., 2014. Fast and accurate water content and T2*mapping in brain tumours localised with FET-PET. Nuclear Instruments & Methods in Physics Research Section a-Accelerators Spectrometers Detectors and Associated Equipment 734, 185–190.
Oros-Peusquens, A.M., Loucao, R., Abbas, Z., Gras, V., Zimmermann, M., Shah, N.J., 2019. A Single-Scan, Rapid Whole-Brain Protocol for Quantitative Water Content Mapping With Neurobiological Implications. Front Neurol 10, 1333.
Parker, G.J.M., Barker, G.J., Tofts, P.S., 2001. Accurate multislice gradient echo T1 measurement in the presence of non-ideal RF pulse shape and RF field nonuniformity. Magn. Reson. Med. 45, 838–845.
Reetz, K., Abbas, Z., Costa, A.S., Gras, V., Tiffin-Richards, F., Mirzazade, S., Holschbach, B., Frank, R.D., Vassiliadou, A., Kruger, T., Eitner, F., Gross, T., Schulz, J.B., Floege, J., Shah, N.J., 2015. Increased cerebral water content in hemodialysis patients. PLoS One 10, e0122188.
Rooney, W.D., Johnson, G., Li, X., Cohen, E.R., Kim, S.G., Ugurbil, K., Springer Jr., C.S., 2007. Magnetic field and tissue dependencies of human brain longitudinal 1H2O relaxation in vivo. Magn. Reson. Med. 57, 308–318.
Shah, N.J., Neeb, H., Kircheis, G., Engels, P., Haussinger, D., Zilles, K., 2008. Quantitative cerebral water content mapping in hepatic encephalopathy. Neuroimage 41, 706–717.
Shah, N.J., Zaitsev, M., Steinhoff, S., Zilles, K., 2001. A new method for fast multislice T-1 mapping. Neuroimage 14, 1175–1185.
Smith, S.M., 2002. Fast robust automated brain extraction. Hum Brain Mapp 17, 143–155.
Steinhoff, S., Zaitsev, M., Zilles, K., Shah, N.J., 2001. Fast T-1 mapping with volume coverage. Magn. Reson. Med. 46, 131–140.
Talairach, J., Tournoux, P., 1988. Co-planar stereotaxic atlas of the human brain: 3-dimensional proportional system: an approach to cerebral imaging. Georg Thieme. Stuttgart, New York.
Tofts, P.S., 2003. PD: Proton Density of Tissue Water. Quantitative Mri of the Brain: Measuring Changes Caused by Disease 85–109.
Volz, S., Noth, U., Jurcoane, A., Ziemann, U., Hattingen, E., Deichmann, R., 2012a. Quantitative proton density mapping: correcting the receiver sensitivity bias via pseudo proton densities. Neuroimage 63, 540–552.
Volz, S., Noth, U., Jurcoane, A., Ziemann, U., Hattingen, E., Deichmann, R., 2012b. Quantitative proton density mapping: correcting the receiver sensitivity bias via pseudo proton densities. Neuroimage 63, 540–552.
Warntjes, J.B., Dahlqvist, O., Lundberg, P., 2007a. Novel method for rapid, simultaneous T1, T2*, and proton density quantification. Magn. Reson. Med. 57, 528–537.
Warntjes, J.B., Dahlqvist, O., Lundberg, P., 2007b. Novel method for rapid, simultaneous T1, T*2, and proton density quantification. Magn Reson Med 57, 528–537.
Weber, H., Paul, D., Elverfeldt, D.V., Hennig, J., Zaitsev, M., 2010. Extended multi-flip-angle B1 mapping: A 3D mapping method for inhomogeneous B1 fields. Concepts in Magnetic Resonance Part B: Magnetic Resonance Engineering 37B, 203–214.
Whittall, K.P., MacKay, A.L., Graeb, D.A., Nugent, R.A., Li, D.K., Paty, D.W., 1997. In vivo measurement of T2 distributions and water contents in normal human brain. Magn. Reson. Med. 37, 34–43.
Wright, I.C., McGuire, P.K., Poline, J.B., Travere, J.M., Murray, R.M., Frith, C.D., Frackowiak, R.S., Friston, K.J., 1995. A voxel-based method for the statistical analysis of gray and white matter density applied to schizophrenia. Neuroimage 2, 244–252.